ADVANCED ENERGY MATERIALS

www.advenergymat.de

Suppressing Li Dendrite Formation in Li_2S-P_2S_5 Solid Electrolyte by LiI Incorporation

*Fudong Han, Jie Yue, Xiangyang Zhu, and Chunsheng Wang**

Solid electrolytes have been considered as a promising approach for Li dendrite prevention because of their high mechanical strength and high Li transference number. However, recent reports indicate that Li dendrites also form in Li_2S-P_2S_5 based sulfide electrolytes at current densities much lower than that in the conventional liquid electrolytes. The methods of suppressing dendrite formation in sulfide electrolytes have rarely been reported because the mechanism for the "unexpected" dendrite formation is unclear, limiting the successful utilization of high-energy Li anode with these electrolytes. Herein, the authors demonstrate that the Li dendrite formation in Li_2S-P_2S_5 glass can be effectively suppressed by tuning the composition of the solid electrolyte interphase (SEI) at the Li/electrolyte interface through incorporating LiI into the electrolyte. This approach introduces high ionic conductivity but electronic insulation of LiI in the SEI, and more importantly, improves the mobility of Li atoms, promoting the Li depositon at the interface and thus suppresses dendrite growth. It is shown that the critical current density is improved significantly after incorporating LiI into Li_2S-P_2S_5 glass, reaching 3.90 mA cm^{-2} at 100 °C after adding 30 mol% LiI. Stable cycling of the Li-Li cells for 200 h is also achieved at 1.50 mA cm^{-2} at 100 °C.

Lithium metal is believed to be the most promising anode due to its extremely high capacity, low density, and the lowest electrode potential.[1,2] However, the utilization of lithium metal anodes with the conventional liquid or polymer electrolytes has not been successful because of the unavoidable lithium dendrite growth which can cause internal short circuit and life-threatening accidents.[3] Solid electrolytes have been considered to be the ideal solution to prevent dendrite growth because of their high shear modulus[4,5] and high Li transference number.[6] In addition, the utilization of nonflammable, inorganic solid electrolytes can also dramatically improve battery safety.[7–9] While various lithium ion conducting materials have been developed, sulfide-based compounds (Li_2S-P_2S_5 and its derivatives) are being considered as one of the most promising solid electrolytes due to their excellent mechanical property (can be densified simply by cold pressing) and high ionic conductivity.[10–12] Unexpectedly, recent reports indicate that the Li dendrites also form in $70Li_2S$-$30P_2S_5$ glass, $75Li_2S$-$25P_2S_5$ glass, $80Li_2S$-$20P_2S_5$ glass-ceramic, and polycrystalline β-Li_3PS_4.[13–15] The formation of Li dendrites leads to rapid short circuit of the Li/electrolyte/Li (Li-Li) cells at current densities larger than 1 mA cm^{-2}.[13,15] It should be noted that even in the conventional liquid electrolyte (1 M $LiPF_6$ in EC/DMC), the lithium metal anode is still able to cycle hundreds of hours at 2 mA cm^{-2} without shorting.[16] This indicates that sulfide electrolytes tend to promote, rather than suppress, dendrite formation when compared with liquid electrolytes. However, until now, there is still no effective approach to suppress the Li dendrite growth in sulfide electrolytes because the mechanism for the "unexpected" dendrite formation is unclear. To the best of our knowledge, there is only one report on the suppression of the lithium dendrite formation in sulfide electrolyte by optimizing the processing conditions.[15] It was shown that hot pressing $75Li_2S$-$25P_2S_5$ solid electrolyte can help to increase the critical current density (at which current the cell will be short circuited by dendrite formation) because of the formation of a highly conductive thio-LISICON phase and the improvement of adhesion between particles. However, the critical current density for the hot-pressed $75Li_2S$-$25P_2S_5$ solid electrolyte is still limited to 1 mA cm^{-2}, much lower than that in the liquid-electrolyte Li batteries. It is fair to conclude that, similar as in the liquid-electrolyte lithium-metal batteries, the main challenge to utilize lithium anode with sulfide solid electrolytes is how to effectively suppress the dendrite formation at a large current.

It has been known that the sulfide solid electrolytes have a limited thermodynamic electrochemical stability window around 1.7–2.1 V.[17–19] Therefore, the interfacial stability between Li metal and sulfide electrolytes is achieved by forming solid electrolyte interphase (SEI) as a passivating layer. The composition of the SEI mainly includes Li_3P, Li_2S, and other Li-containing compounds depending on the composition of the electrolyte.[17,18,20–22] Since the Li dendrites have to grow through the SEI, the composition of the SEI should play an important role in the dendrite formation. It is therefore hypothesized that the dendrite formation in sulfide electrolytes can be suppressed by tuning the composition of the electrolyte.

In this work, we demonstrated that the formation of Li dendrites in Li_2S-P_2S_5 glass can be suppressed by incorporating LiI into the electrolyte. Our interest in glass-type electrolyte

F. Han, J. Yue, X. Zhu, Prof. C. Wang
Department of Chemical and Biomolecular Engineering
University of Maryland
College Park, MD 20740, USA
E-mail: cswang@umd.edu

The ORCID identification number(s) for the author(s) of this article can be found under https://doi.org/10.1002/aenm.201703644.

DOI: 10.1002/aenm.201703644

originates from its two fundamental attributes: the absence of highly resistive grain boundaries and the high flexibility to tune its composition. LiI was chosen as the additive because both the ionic conductivity[23–26] and the electrochemical stability of sulfide electrolytes can be improved after LiI incorporation.[27–30] In addition, incorporating LiI into Li_2S-P_2S_5 glass can also introduce highly ionic conductive but electronic insulating LiI in the SEI,[18,21] and more importantly, improve the mobility of Li atoms at the Li/electrolyte interface,[31,32] suppressing the dendrite growth. Our results show that the critical current density was improved significantly after introducing LiI into Li_2S-P_2S_5 glass electrolyte, reaching 3.90 mA cm^{-2} at 100 °C after adding 30 mol% LiI. Stable cycling of the Li-Li symmetrical cells for 200 h was also achieved at 1.50 mA cm^{-2} with a charge/discharge capacity of 1.5 mA h cm^{-2} at 100 °C.

Different amount of LiI was introduced into Li_2S-P_2S_5 glass electrolytes by high-energy ball-milling of Li_2S, P_2S_5, and LiI at the compositions of $(100-x)(0.75Li_2S\text{-}0.25P_2S_5)-xLiI$ (mol%), where x = 0, 10, 20, 30, and 40. **Figure 1**a shows the X-ray diffraction (XRD) patterns of as-prepared $(100-x)(0.75Li_2S\text{-}0.25P_2S_5)-xLiI$ glass electrolytes. All the solid electrolytes have amorphous structure except the sample with 40 mol% LiI addition wherein some unknown crystalline phases were formed after ball-milling. No apparent change could be observed from the Raman spectra (Figure 1b) after introducing different amounts of LiI into the Li_2S-P_2S_5 electrolytes. More importantly, no LiI can be detected from XRD and Raman spectra, indicating that LiI has been successfully dissolved into the electrolytes. Figure 1c shows the deconvoluted Raman spectra in a specified region. The peaks at around 421, 404, and 386 cm^{-1} can be attributed to PS_4^{3-}, $P_2S_7^{4-}$, and $P_2S_6^{4-}$ in the glass electrolytes, respectively.[33] The relative ratio of these peaks does not change much after introducing different amounts of LiI in Li_2S-P_2S_5 (Table S1, Supporting Information), indicating that the local structure around phosphorus of these glasses does not change by LiI incorporation, consistent with the previous reports.[23,24,34]

We evaluated the dendrite suppression capability of $(100-x)(0.75Li_2S\text{-}0.25P_2S_5)-xLiI$ (x = 0, 10, 20, 30, and 40) glass electrolytes by galvanostatic cycling of Li-Li cells at step-increased current densities at 25 °C. **Figure 2**a–e shows the voltage-time profiles for solid electrolytes with different amounts of LiI incorporation. Initially, the voltages increased with currents for all solid electrolytes, and the magnitudes of the voltage at the same current follow the trend: $x = 0 > x = 10 > x = 20 > x = 40 > x = 30$, consistent with the ionic conductivity of the solid electrolytes (Figure S1, Supporting Information). After cycling for a certain amount of time, all of the Li-Li cells experienced a voltage drop. The voltage drop is considered as a result of lithium dendrite formation in the solid electrolytes, as can be observed from the backscattering electron images and the elemental mappings of the cross-section of electrolyte after cycling (Figures S2 and S3, Supporting Information). The current density at which voltage dropped is considered as the critical current density for the Li dendrite formation in electrolyte, and the magnitude of the critical current density is used to evaluate the capability of dendrite suppression.[35–37] Figure 2f compares the critical current densities for the electrolytes with different LiI contents. The critical current density for the $0.75Li_2S\text{-}0.25P_2S_5$ (LPS) glass electrolyte without LiI addition is determined to be 0.40 mA cm^{-2}. The critical current density increases with increasing the content of LiI, reaching the maximum value of 1.00 mA cm^{-2} (corresponding to a 150% increase) at x = 30 (LPS30I), and then decreases to 0.35 mA cm^{-2} at x = 40. The reason for the decreased critical current density at x = 40 is still not clear, but it may be related to the unknown impurities in the electrolyte as demonstrated in Figure 1a. The critical current density of LPS30I is much higher than the reported critical current densities of garnet-type $Li_7La_3Zr_2O_{12}$ solid electrolytes.[36–39]

As high temperature operation is one important advantage for all-solid-state lithium batteries, the effects of temperature on the critical current densities of LPS and LPS30I were also investigated. **Figure 3** shows the galvanostatic cycling of the Li/LPS/Li and Li/LPS30I/Li cells at 60 and 100 °C. The critical current density for LPS is 0.88 mA cm^{-2} at 60 °C and 2.40 mA cm^{-2} at 100 °C, while the critical current density for LPS30I is 2.16 mA cm^{-2} at 60 °C and 3.90 mA cm^{-2} at 100 °C.

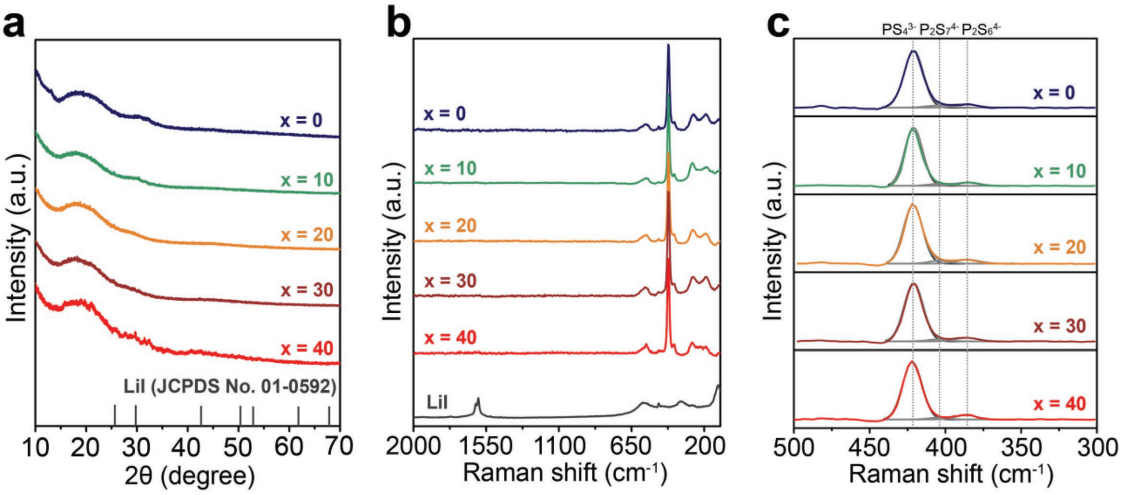

Figure 1. a) XRD patterns, b) Raman spectra, and c) deconvoluted Raman spectra of $(100-x)(0.75Li_2S\text{-}0.25P_2S_5)-xLiI$, where x = 0, 10, 20, 30, and 40. The XRD pattern and Raman spectrum of LiI are also included as a reference.

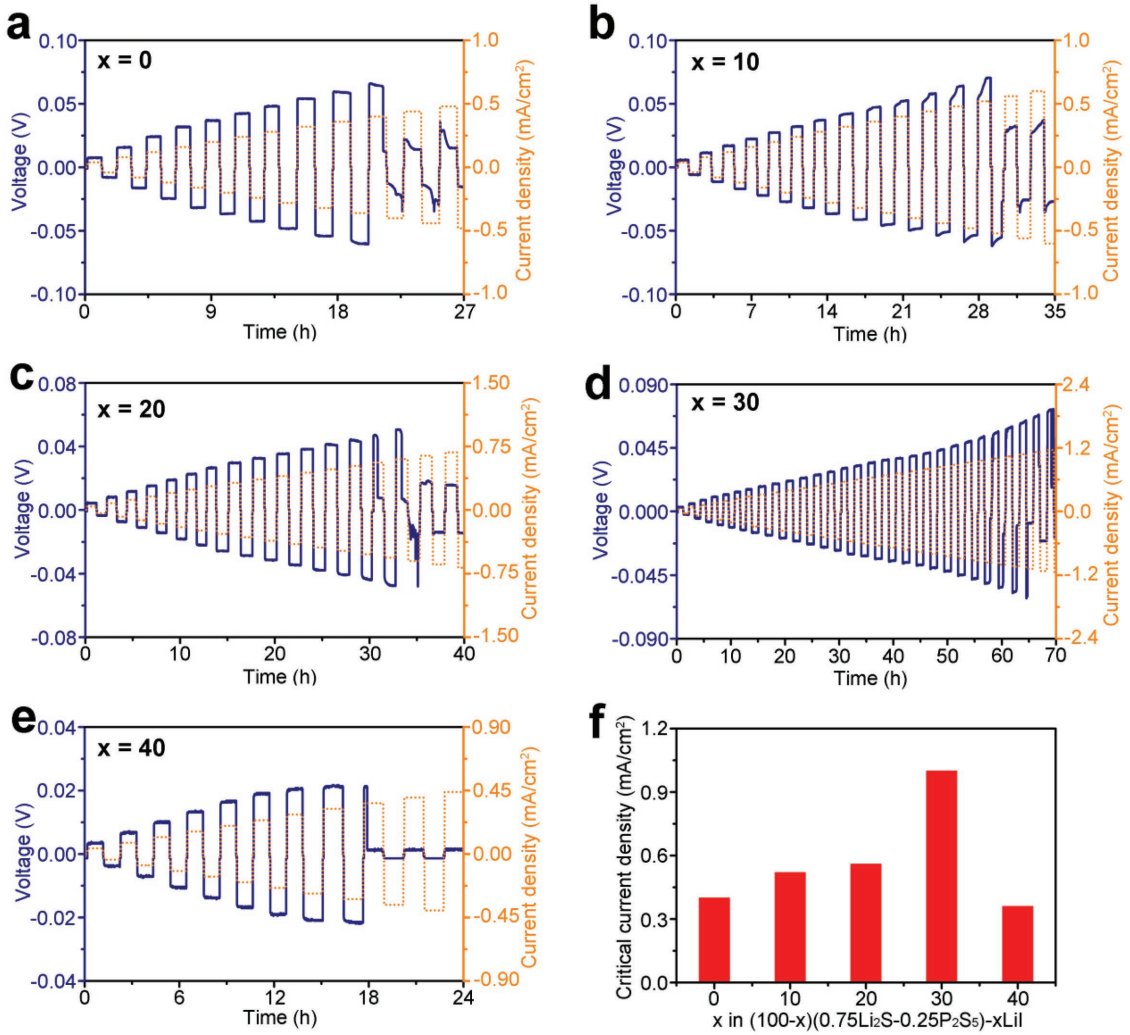

Figure 2. Galvanostatic cycling of the Li-Li cells at step-increased current densities at 25 °C with $(100 - x)(0.75Li_2S\text{-}0.25P_2S_5) - xLiI$ electrolytes, where a) $x = 0$, b) $x = 10$, c) $x = 20$, d) $x = 30$, and e) $x = 40$. The time for each charge and discharge is 1 h. The step size for the current increase is 0.04 mA cm^{-2}. f) The critical current densities versus the composition of the sulfide electrolytes.

The critical current densities of both LPS and LPS30I increase with increasing temperature, a trend consistent with the previous report on the dendrite formation in $Li_7La_3Zr_2O_{12}$.[35,36] However, the increase in critical current density of LPS30I is much more significant than that of LPS, and 3.9 mA cm^{-2} is the highest critical current density that has been reported so far for Li cycling with sulfide electrolytes.

It should be noted that the exact value for the critical current density depends on experimental setup such as the step size for the increase of current and the capacity for each charge and discharge. Ideally, the step size should be as small as possible to get the most accurate critical current density. This explains why the critical current density of $75Li_2S\text{-}25P_2S_5$ glass electrolyte measured in this work (step size: 0.04 mA cm^{-2}) is much smaller than that in the previous work (step size: 0.5 mA cm^{-2}).[15] Nevertheless, the critical current density of different electrolytes tested under the same condition can be used to compare their capabilities for dendrite suppression.[15,35–37,39,40] The obtained values for the critical current densities in this work are reproducible from another set of experiment (Figures S4 and S5, Supporting Information), and we estimate the error from different measurements is less than 10%.

We then compared the cycling performances of the Li/LPS/Li and Li/LPS30I/Li cells at different temperatures. **Figure 4**a shows the voltage profile of the Li/LPS/Li cell cycled at 0.3 mA cm^{-2} at 25 °C. The voltage of the cell seems to be stable for 9 cycles, and then suddenly drops at the 10th cycle (around 20 h). The voltage drop is considered to be a result of the soft-shorting by formation of dendrites in the electrolyte,[1] as supported by the electrochemical impedance spectroscopy (EIS) result of the cell after cycling for 64 h (Figure S6, Supporting Information). The voltage was then stabilized at around 0.006 V in the following cycles. The nonzero voltage after short-circuit implies the nonzero resistance of the dendrites.[41] The short-circuit of the Li/LPS/Li cells can also be observed, within 60 h, when it was cycled at 0.6 mA cm^{-2} at 60 °C and 1.5 mA cm^{-2} at 100 °C. However, all the three Li/LPS30I/Li cells were able to stably cycle for more than 200 h at the same currents and at the same temperatures as the Li/LPS/Li cells. In addition, the feasibility of using LPS30I electrolyte with Li metal was

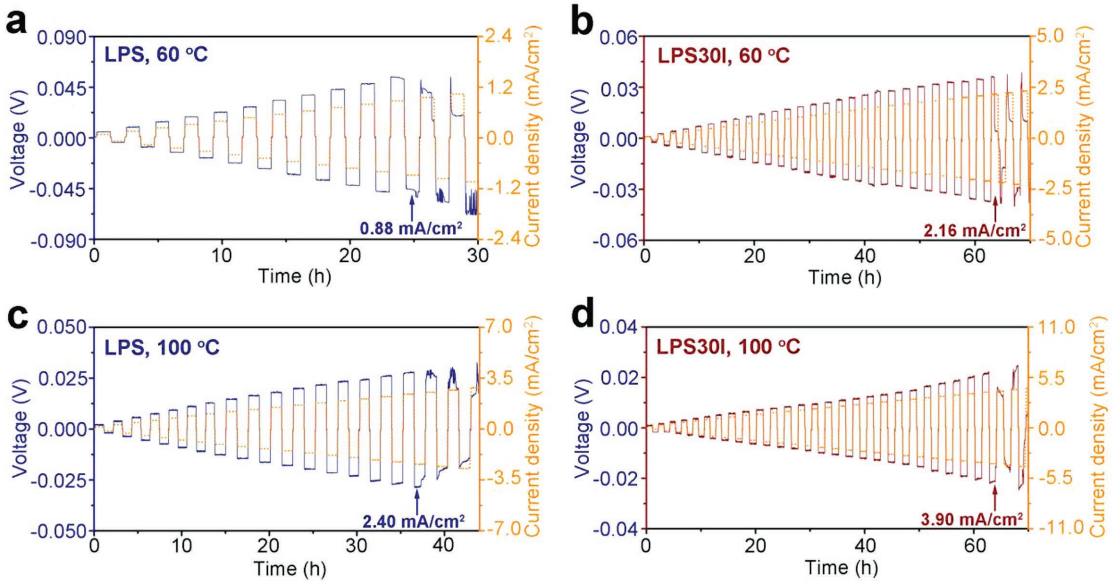

Figure 3. Galvanostatic cycling of the Li/LPS/Li and Li/LPS30I/Li cells at step-increased current densities at a,b) 60 °C and c,d) 100 °C. The time for each charge and discharge is 1 h. The step sizes for the current increase are 0.08 mA cm^{-2} at 60 °C and 0.15 mA cm^{-2} at 100 °C.

also demonstrated in a full cell with an $LiNbO_3$-coated $LiCoO_2$ ($LiCoO_2$@$LiNbO_3$) cathode. Such an Li/LPS30I/$LiCoO_2$@$LiNbO_3$ full cell can be charged/discharged for more than 40 cycles with a capacity around 102 mA h g^{-1} (corresponding to 0.91 mA h cm^{-2}) at 0.2 C (corresponding to 0.25 mA cm^{-2}) at 25 °C (Figure S7, Supporting Information). The stable cycling of the Li/LPS30I/$LiCoO_2$@$LiNbO_3$ full cell also implies the great anodic stability of the LPS30I electrolyte.

All of the above results indicate the dendrite suppression capability of Li_2S-P_2S_5 electrolytes could be significantly enhanced

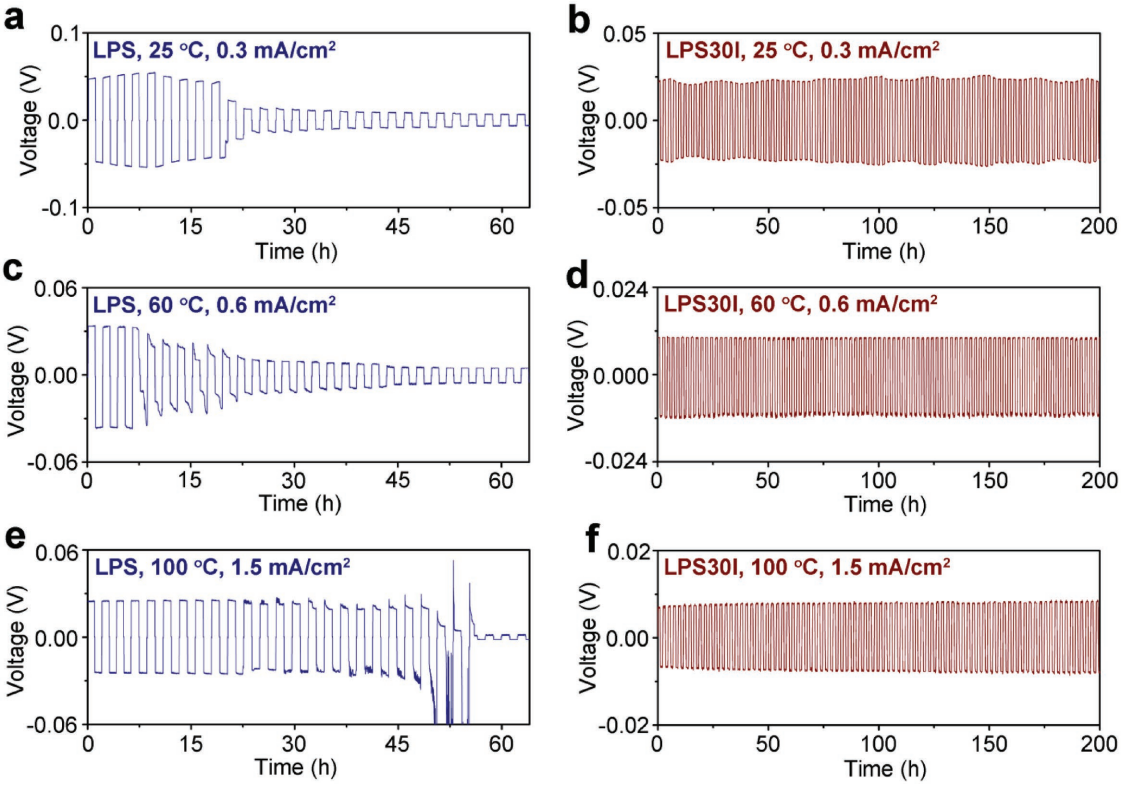

Figure 4. Galvanostatic cycling of the Li/LPS/Li and Li/LPS30I/Li cells at constant current densities at a,b) 25 °C, c,d) 60 °C, e,f) and 100 °C. The time for each charge and discharge is 1 h.

by LiI incorporation, and LPS30I glass can be used as a promising electrolyte with Li metal anode. The exact mechanism about such a significant improvement is not fully understood but could be related with the introduction of LiI in the SEI at the Li/electrolyte interface. Both theoretical and experimental works have demonstrated that LPS will be decomposed into Li_2S and Li_3P (with a molar ratio of 1/4), while LPS30I will be decomposed into Li_2S, Li_3P, and LiI (with a molar ratio of 7/28/6) when contacting with Li.[17,18,20,21] The formation of LiI was also confirmed from the Raman spectra of the Li disc detached from the Li/LPS30I/Li after cycling (Figure S8, Supporting Information). The formation of LiI at the Li/electrolyte interface can improve the ionic conductivity of SEI, and more importantly improve the mobility of Li atoms,[31,32] promoting the Li deposition at the interface and thus suppressing the dendrite growth. In addition, introducing LiI in the SEI also helps to lower the electronic conductivity of SEI based on the larger bandgap of LiI (6.4 eV)[42] than that of Li_3P (0.7 eV),[43] although the formation of nonstoichiometric LiI may also slightly increase the electronic conductivity.[44,45] Although all lithium halides have been reported to be able to improve the surface mobility of Li atoms[31] and reduce the electronic conductivity, the critical current densities of the Li_2S-P_2S_5 electrolytes after the incorporations of LiF, LiCl, and LiBr are much smaller than that of LPS30I (Figure S9, Supporting Information), possibly due to the limited solubilities of LiF, LiCl, and LiBr in Li_2S-P_2S_5 glass. Nevertheless, it should be noted that the dendrite suppression capability may also be influenced by other factors, such as the microstructure of electrolyte,[37,38] defects,[14] mechanical, and electrical properties of the solid electrolyte especially around the particle boundaries.[46] Further work is needed to elucidate the effect of LiI incorporation on these variables to gain a better understanding of the mechanism.

In summary, we demonstrate that the incorporation of LiI into the Li_2S-P_2P_5 glass electrolytes can effectively improve the dendrite suppression capability, and the $70(0.75Li_2S\text{-}0.25P_2S_5)$-30LiI (LPS30I) electrolyte exhibits the highest capability for dendrite suppression. The critical current density of LPS30I reaches 3.90 mA cm^{-2} at 100 °C, and the Li/LPS30I/Li cell could cycle 200 h at 1.50 mA cm^{-2} at 100 °C, representing the best performance for Li cycling with sulfide electrolyte reported to date. This work provides a viable strategy to suppress the dendrite formation in inorganic solid electrolyte by tuning the composition of SEI at the Li/electrolyte interface.

Experimental Section

Synthesis: $(100-x)(0.75Li_2S\text{-}0.25P_2S_5)-xLiI$ ($x = 0$, 10, 20, 30, and 40) solid electrolytes were synthesized using high-energy mechanical milling.[24,25] Li_2S (Sigma-Aldrich, 99.98%), P_2S_5 (Sigma-Aldrich, 99%), and LiI (Sigma-Aldrich, 99.99%) were used as starting materials. These materials were weighed based on the molar ratios of $Li_2S/P_2S_5/LiI$ in an argon-filled glovebox, subjected to a zirconia ceramic vial, and ball-milled (PM 100, Retsch) at 500 rpm for 10 h.

Characterization: Powder X-ray diffraction patterns were obtained with a D8 Advance with LynxEye and SolX (Bruker AXS, WI, USA) using Cu Kα radiation. The morphologies of the sample were examined using a Hitachi SU-70 field-emission scanning electron microscope. Raman spectra were measured on a Horiba Jobin Yvon Labram Aramis using a 532 nm diode-pumped solid-state laser.

Electrochemistry: To assemble the Li/electrolyte/Li cell, 180 mg solid electrolyte powder was pressed into a pellet under 360 MPa in a polytetrafluoroethylene (PTFE) tank with a diameter of 10 mm. After that, two 45 µm thick Li discs with a diameter of 10 mm were attached on both sides of the solid electrolyte. The formed Li/electrolyte/Li cell was then sandwiched between two stainless steel rods which function as current collectors. For the assembly of the all-solid-state full cells, $LiNbO_3$-coated $LiCoO_2$ ($LiCoO_2$@$LiNbO_3$) was mixed with LPS30I glass electrolyte with a weight ratio of 70:30 to prepare the cathode composite. The cathode composite (10 mg) was put on the top of the LPS30I glass electrolyte (150 mg) and cold pressed together under 360 MPa in a PTFE tank with a diameter of 10 mm. After that, a 45 µm thick Li metal was attached on the other side of the LPS30I layer as a counter and reference electrode. The formed three-layered pellet was then cold pressed under 120 MPa between two stainless steel rods which function as current collectors. The Li/electrolyte/Li and Li/LPS30I/$LiCoO_2$@$LiNbO_3$ cells were rested for 6 h prior to test to stabilize the interface between Li and electrolyte. No formation cycles at small currents were used in this work.[35] The ionic conductivity of the solid electrolytes was measured from the EIS test of the Pt/electrolyte/Pt cell at room temperature. All the electrode preparation and cell assembly processes were performed in the glovebox. The galvanostatic cycling charge/discharge behavior was tested at different temperatures using an Arbin BT2000 workstation (Arbin Instruments, TX, USA). The time for each charge (and discharge) is 1 h. The electrochemical impedance spectrum was measured on an electrochemistry workstation (Solartron 1287/1260).

Supporting Information

Supporting Information is available from the Wiley Online Library or from the author.

Acknowledgements

F.H. and J.Y. contributed equally to this work. The authors acknowledge the insightful discussions with Dr. Ping Liu (University of California, San Diego) and Dan Addison (Liox Power, Inc.). This work was supported by the U.S. Department of Energy ARPA-E (Award No. DE-AR0000781). The authors also thank the support of the Maryland Nanocenter and its AIMLab.

Conflict of Interest

The authors declare no conflict of interest.

Keywords

all-solid-state batteries, dendrites, glass, Li anodes, solid electrolytes

Received: December 26, 2017
Revised: January 22, 2018
Published online:

[1] P. Albertus, S. Babinec, S. Litzelman, A. Newman, *Nat. Energy* **2018**, *3*, 16.
[2] K. Zhang, G. H. Lee, M. Park, W. J. Li, Y. M. Kang, *Adv. Energy Mater.* **2016**, *6*, 1600811.
[3] J. M. Zheng, P. F. Yan, D. H. Mei, M. H. Engelhard, S. S. Cartmell, B. J. Polzin, C. M. Wang, J. G. Zhang, W. Xu, *Adv. Energy Mater.* **2016**, *6*, 1502151.
[4] C. Monroe, J. Newman, *J. Electrochem. Soc.* **2005**, *152*, A396.

[5] D. Zhou, R. L. Liu, Y. B. He, F. Y. Li, M. Liu, B. H. Li, Q. H. Yang, Q. Cai, F. Y. Kang, *Adv. Energy Mater.* **2016**, *6*, 1502214.
[6] C. Brissot, M. Rosso, J. N. Chazalviel, S. Lascaud, *J. Power Sources* **1999**, *81*, 925.
[7] J. C. Li, C. Ma, M. F. Chi, C. D. Liang, N. J. Dudney, *Adv. Energy Mater.* **2015**, *5*, 1401408.
[8] J. Janek, W. G. Zeier, *Nat. Energy* **2016**, *1*, 16141.
[9] J. van den Broek, S. Afyon, J. L. M. Rupp, *Adv. Energy Mater.* **2016**, *6*, 1600736.
[10] A. Sakuda, A. Hayashi, M. Tatsumisago, *Sci. Rep.* **2013**, *3*, 2261.
[11] Y. Kato, S. Hori, T. Saito, K. Suzuki, M. Hirayama, A. Mitsui, M. Yonemura, H. Iba, R. Kanno, *Nat. Energy* **2016**, *1*, 16030.
[12] D. Y. Oh, Y. J. Nam, K. H. Park, S. H. Jung, S. J. Cho, Y. K. Kim, Y. G. Lee, S. Y. Lee, Y. S. Jung, *Adv. Energy Mater.* **2015**, *5*, 1500865.
[13] M. Nagao, A. Hayashi, M. Tatsumisago, T. Kanetsuku, T. Tsuda, S. Kuwabata, *Phys. Chem. Chem. Phys.* **2013**, *15*, 18600.
[14] L. Porz, T. Swamy, B. W. Sheldon, D. Rettenwander, T. Frömling, H. L. Thaman, S. Berendts, R. Uecker, W. C. Carter, Y. M. Chiang, *Adv. Energy Mater.* **2017**, *7*, 1701003.
[15] R. Garcia-Mendez, F. Mizuno, R. G. Zhang, T. S. Arthur, J. Sakamoto, *Electrochim. Acta* **2017**, *237*, 144.
[16] E. Markevich, G. Salitra, F. Chesneau, M. Schmidt, D. Aurbach, *ACS Energy Lett.* **2017**, *2*, 1321.
[17] F. D. Han, Y. Z. Zhu, X. F. He, Y. F. Mo, C. S. Wang, *Adv. Energy Mater.* **2016**, *6*, 1501590.
[18] Y. Zhu, X. He, Y. Mo, *ACS Appl. Mater. Interfaces* **2015**, *7*, 23685.
[19] F. D. Han, T. Gao, Y. J. Zhu, K. J. Gaskell, C. S. Wang, *Adv. Mater.* **2015**, *27*, 3473.
[20] S. Wenzel, D. A. Weber, T. Leichtweiss, M. R. Busche, J. Sann, J. Janek, *Solid State Ionics* **2016**, *286*, 24.
[21] S. Wenzel, S. J. Sedlmaier, C. Dietrich, W. G. Zeier, J. Janek, *Solid State Ionics* **2017**, https://doi.org/10.1016/j.ssi.2017.07.005.
[22] S. Wenzel, S. Randau, T. Leichtweiss, D. A. Weber, J. Sann, W. G. Zeier, J. Janek, *Chem. Mater.* **2016**, *28*, 2400.
[23] R. Mercier, J. P. Malugani, B. Fahys, G. Robert, *Solid State Ionics* **1981**, *5*, 663.
[24] S. Ujiie, A. Hayashi, M. Tatsumisago, *Solid State Ionics* **2012**, *211*, 42.
[25] S. Ujiie, A. Hayashi, M. Tatsumisago, *J. Solid State Electrochem.* **2013**, *17*, 675.
[26] K. Takada, T. Inada, A. Kajiyama, H. Sasaki, S. Kondo, M. Watanabe, M. Murayama, R. Kanno, *Solid State Ionics* **2003**, *158*, 269.
[27] E. Rangasamy, Z. C. Liu, M. Gobet, K. Pilar, G. Sahu, W. Zhou, H. Wu, S. Greenbaum, C. D. Liang, *J. Am. Chem. Soc.* **2015**, *137*, 1384.
[28] S. J. Sedlmaier, S. Indris, C. Dietrich, M. Yavuz, C. Draeger, F. von Seggern, H. Sommer, J. Janek, *Chem. Mater.* **2017**, *29*, 1830.
[29] Y. Aihara, S. Ito, R. Omoda, T. Yamada, S. Fujiki, T. Watanabe, Y. Park, S. Doo, *Front. Energy Res.* **2016**, *4*, 18.
[30] P. Bron, B. Roling, S. Dehnen, *J. Power Sources* **2017**, *352*, 127.
[31] Y. Y. Lu, Z. Y. Tu, L. A. Archer, *Nat. Mater.* **2014**, *13*, 961.
[32] L. Ma, M. S. Kim, L. A. Archer, *Chem. Mater.* **2017**, *29*, 4181.
[33] C. Dietrich, D. A. Weber, S. J. Sedlmaier, S. Indris, S. P. Culver, D. Walter, J. Janek, W. G. Zeier, *J. Mater. Chem. A* **2017**, *5*, 18111.
[34] N. H. H. Phuc, E. Hirahara, K. Morikawa, H. Muto, A. Matsuda, *J. Power Sources* **2017**, *365*, 7.
[35] A. Sharafi, H. M. Meyer, J. Nanda, J. Wolfenstine, J. Sakamoto, *J. Power Sources* **2016**, *302*, 135.
[36] C. L. Tsai, V. Roddatis, C. V. Chandran, Q. Ma, S. Uhlenbruck, M. Bram, P. Heitjans, O. Guillon, *ACS Appl. Mater. Interfaces* **2016**, *8*, 10617.
[37] L. Cheng, W. Chen, M. Kunz, K. Persson, N. Tamura, G. Chen, M. Doeff, *ACS Appl. Mater. Interfaces* **2015**, *7*, 2073.
[38] A. Sharafi, C. G. Haslam, R. D. Kerns, J. Wolfenstine, J. Sakamoto, *J. Mater. Chem. A* **2017**, *5*, 21491.
[39] R. H. Basappa, T. Ito, T. Morimura, R. Bekarevich, K. Mitsuishi, H. Yamada, *J. Power Sources* **2017**, *363*, 145.
[40] J. Wakasugi, H. Munakata, K. Kanamura, *J. Electrochem. Soc.* **2017**, *164*, A1022.
[41] M. Rosso, T. Gobron, C. Brissot, J. N. Chazalviel, S. Lascaud, *J. Power Sources* **2001**, *97*, 804.
[42] Y. M. Gao, Y. F. Jiang, N. P. Wang, *Phys. B* **2014**, *447*, 47.
[43] S. N. Wu, S. S. Neo, Z. L. Dong, F. Boey, P. Wu, *J. Phys. Chem. C* **2010**, *114*, 16706.
[44] C. C. Liang, J. Epstein, G. H. Boyle, *J. Electrochem. Soc.* **1969**, *116*, 1452.
[45] S. D. Jones, J. R. Akridge, F. K. Shokoohi, *Solid State Ionics* **1994**, *69*, 357.
[46] S. Yu, R. D. Schmidt, R. Garcia-Mendez, E. Herbert, N. J. Dudney, J. B. Wolfenstine, J. Sakamoto, D. J. Siegel, *Chem. Mater.* **2016**, *28*, 197.